Hydrogenated Polybutadiene Morphology and Its Effects on Small Molecule Diffusion

P. Y. Furlan*

Bell Communications Research, 331 Newman Springs Road, Red Bank, New Jersey 07701

Received November 13, 1991; Revised Manuscript Received July 15, 1992

ABSTRACT: The transport behavior of *n*-decyl alcohol ($C_{10}OH$) into hydrogenated polybutadienes (HPBD) (MW = 100 000; $M_w/M_n < 1.1$) with varied branch contents was investigated using a FTIR–attenuated total reflection sampling method. Film samples were solution cast onto the ZnSe ATR element, and the residual solvent was removed by annealing the samples at 80 °C for 12 h. The polymer films were characterized by FTIR, calorimetry, density and optical microscopy. A significant difference in crystallinities determined by DSC and density measurements was evident. A nonlinear dependence of the equilibrium sorption on the density of HPBDs was observed, and an exponential dependence of the diffusant diffusivities on the density of the polymers was found. The observed transport behaviors deviate from those predicted using a simple two-phase model. The source for the deficiency of the two-phase model in modeling diffusion experiments may be due to the presence of a partially ordered region, although other possible sources, such as sample swelling, a rapid change in the polymer–solvent interactions at high branch content, or the exclusion of important variables in modeling, may account for the disagreement of our data with the simple two-phase model.

Introduction

Because most polyolefins contain additives and stabilizers, the transport of small molecules in polyolefins is an important scientific and practical issue. For example, polyolefin insulated conductor (PIC) cable, an important component in the telephone network, is stabilized by various additives, and the loss of the stabilizer by diffusion processes causes premature failure of the cable. Predictions of the cable's useful lifetime from accelerated aging tests need to be augmented by a fundamental understanding of the mechanisms of stabilizer loss.

In a previous paper,[1] we showed that infrared spectroscopy, in combination with an attenuated total reflection (ATR) liquid cell, can be used as an in situ probe of small molecule diffusion in semicrystalline polyolefins. By recording the real-time intensity of IR bands from diffusant molecules, one can measure the diffusion kinetics and determine the diffusion coefficients. Our previous study[1] showed that the diffusion of linear alcohol in branched polyethylenes obeys a classic Fickian model.[2]

Two-Phase Model. The transport properties, i.e., the permeability and the diffusivity, of small molecules in semicrystalline polyolefins are influenced by the degree of crystallinity in polymers, decreasing as the crystallinity increases.[3] A two-phase model, where the polyolefin contains distinct amorphous and crystalline regions, has been used to explain this phenomenon.[4-11,41,42] Due to the tight packing of molecular chains in the crystalline phase, diffusants dissolve and travel only in the amorphous region.[4,5] The two-phase model was first proposed by Michaels et al.[4,5] in a study of the solubility of gases in polyethylenes. To better correlate diffusivity with crystallinity, a "geometric impedance factor", τ, was introduced to explain diffusion, much as the flow of gases through porous media or electric current through a composite of nonconducting and conducting phases. Figure 1 shows schematically how the geometric impedance factor affects the diffusion of small molecules through a semicrystalline polymer matrix.[6,7] Increases in crystallinity cause an increase in the path length, or "tortuosity", between points "a" and "b"; also shown are "blocking" effects, where small molecules are unable to pass through point "c".[6,7] However, the reduction in diffusion rates predicted by the modified model was too small to match the experimental gas diffusion results.[11-13,43,44]

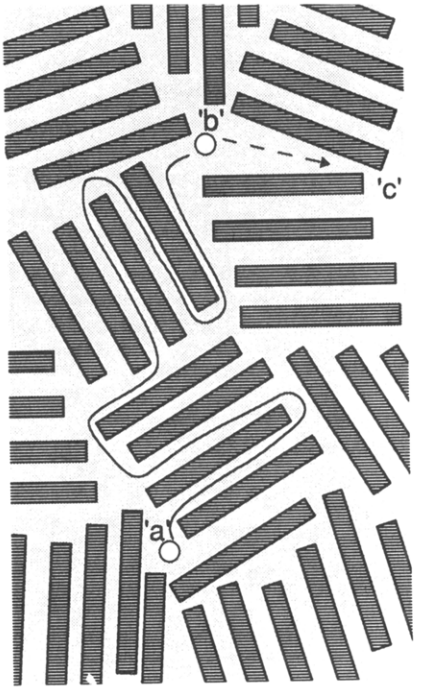

Figure 1. Schematic representation of the two-phase model, which shows the "detour" and "blocking" effects, or the "geometric impedance", of crystals on the transport of small molecules through a semicrystalline polymer matrix. An increase in crystallinity results in an increase in the path length between points "a" and "b"; because of the crystal "blocking", small molecule are unable to pass through point "c".[6,7]

To further reduce the calculated diffusivity in semicrystalline polyethylenes, Michaels and Parker[4] proposed a "chain immobilization factor", β, that accounts for changes in the properties of the amorphous region caused by the existence of the crystallites. They considered an activated diffusion process involving the cooperative movement of amorphous chain segments and diffusion

* Current address: 500 Jimmy Ann Dr., Apt. 222, Daytona Beach, FL 32114.

0024-9297/92/2225-6516$03.00/0 © 1992 American Chemical Society

Table I
Physical Properties for n-Decyl Alcohol Diffusing in Hydrogenated Polybutadienes of Varying Ethyl Branch Content

branch content		DSC			density column (23 °C)			diffusive behavior (25 °C)	
x_{12}	n_b (per 100 C)	T_m (°C)	ΔH_f (cal/g)	X_c	ρ_a* (g/cm³)	ρ (g/cm³)	X_c	10^9D (cm²/s)	I_s (arbitrary)
0.20	6	105	30.78	0.46	0.857	0.942	0.63	0.013	40
0.24	7	101	29.24	0.44	0.857	0.928	0.53	0.027	41
0.36	11	95	23.08	0.35	0.858	0.916	0.44	0.055	44
0.65	24				0.863	0.895	0.26	0.22	118
0.93	44				0.869	0.885	0.14	0.4	270

[a] Krigas et al.[38]

molecules. The mobility of polymer chains is restricted by the cross-linking action of crystallites, and thus the diffusant constant is reduced. With this modification, the effective diffusion constant is given by $D = D_a/\tau\beta$, where D_a is the diffusion constant in amorphous polyethylene; τ is dependent on the size, shape, and distribution of crystallites in the polymer matrix but not on the size and/or shape of the diffusants, while β depends not only on the size, shape, and distribution of the crystallites in the polymer matrix but also on the size and/or shape of the diffusants. Even with these modifications, a satisfactory correlation between diffusant diffusivity and crystallinity in semicrystalline polyolefins has not been found.[3]

In the present work, we used FTIR–ATR sampling methods to investigate the diffusive behavior of small molecules as a function of morphology for a series of hydrogenated polybutadienes (HPBD). These polymers are essentially polyethylenes with ethyl side branches, varying from 6 to 44 branches/100 backbone carbons. To understand how morphological changes affect the transport properties of small molecules in polymers, FTIR, calorimetry, density, and optical microscopy techniques were used to characterize the branch content, crystallinity, and morphology of the polymer samples.

Experimental Section

Materials and Material Characterization. The polymers were custom synthesized by anionic polymerization of butadiene by Scientific Polymer Products, Inc. The samples has molecular weights of approximately 100 000 and polydispersities of less than 1.1. The 1,2-vinyl content of the polybutadiene was controlled by the addition of a small amount of tetrahydrofuran during the polymerization, and the overall vinyl content was characterized by infrared spectroscopy using the vinyl vibration band at 972 cm^{-1}. The branch contents are reported as x_{12} and n_b, where x_{12} is the mole fraction of 1,2 addition during polymerization and n_b is the number of ethyl branches per 100 backbone carbons.[38] The polybutadienes were converted to their saturated analogs by hydrogenation. No changes in branch content were observed.

To eliminate contact problems during ATR measurements, film samples were solvent cast onto the ZnSe ATR elements. The polymer solution, approximately 2% by weight, was prepared by dissolving the hydrogenated polybutadiene in cyclohexane at 70 °C. The polymer solution was poured over the sampling surface of a prewarmed ATR crystal, and the residual solvent was removed by placing the film in a nitrogen-purged oven for 12 h at 80 °C. The FTIR–ATR spectrum did not show any detectable residual solvent.

Melting temperatures were determined with a Perkin-Elmer Model DSC-2 differential scanning calorimeter, calibrated with indium and $C_{34}H_{69}$, at a heating rate of 10 °C/min. The reported melting temperatures correspond to the maxima of the endothermic peaks. The measured enthalpies of fusion were converted to the degree of crystallinity X_c by taking 66.29 cal/g as the enthalpy of fusion of the perfect polyethylene crystal.[39]

Densities of the film samples were measured at 23 °C by a density gradient column filled with a mixture of isopropyl alcohol and distilled water covering the range of densities from 0.790 to 1.000 g/cm³. To convert the measured densities to the degree of crystallinity, the following equation, based on a two-phase model, was used:

$$X_c = \left(\frac{\rho_a - \rho}{\rho_a - \rho_c}\right)\left(\frac{\rho_c}{\rho}\right)$$

where ρ is the density of the sample, ρ_c is the density of the crystalline phase (1.000 cm³/g), and ρ_a is the density of the amorphous phase. The density of the amorphous phase in highly branched HPBD samples depends on the branch content,[38] and thus the literature values for the amorphous densities, listed in Table I, were used to calculate the degree of crystallinity.

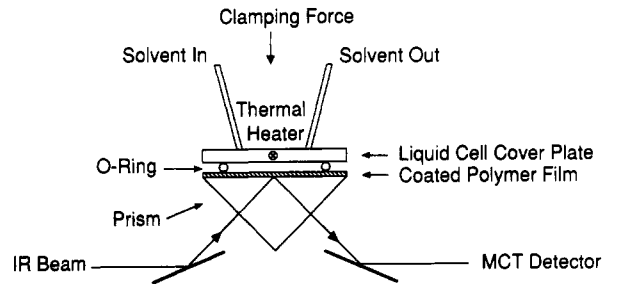

Figure 2. Schematic of the optical path and the arrangement of a single reflection ATR liquid cell attachment (Harrick Scientific Corp.). The liquid cell consists of a 45° ZnSe prism and an O-ring-sealed cover plate with two luer lock fittings, which are held together by a cover clamp. The pure solvent spectrum was obtained by injecting solvent directly onto the sample surface of the ZnSe prism. For the diffusion measurement, a polymer thin film was first coated on the sampling surface of the prism, the solvent was then injected into the cell, and the selected solvent was recorded as a function of time.

The gross morphology of the samples was examined using a Carl Zeiss UltraPhot III polarized optical microscope with transmitted light at magnifications between 200 and 800. The photomicrographs were taken at a magnification of 200 where the numerical aperture of the optical lens was 0.22 and the depth of field was 11.1 μm at 550 nm.

FTIR–ATR Measurements. Infrared spectra were collected using a Fourier transform infrared spectrometer (FTIR, Bomem Model DA3). The spectrometer is equipped with a liquid-nitrogen-cooled, narrow-band MCT detector and a single reflection ATR liquid cell accessory (Harrick Scientific Corp.). The liquid cell consists of a 45° ZnSe prism and an O-ring-sealed cover plate. The cell arrangement and the optical path are illustrated in Figure 2. Details of the method are given in ref 1. All ATR spectra were collected at 2-cm^{-1} resolution with 50 scans coadded in 1 min for each data point. The diffusant for these experiments was n-decyl alcohol. The pure solvent spectrum was obtained by injecting the solvent directly onto the sampling surface of the ZnSe prism. For diffusion measurements, the polymer thin film was first coated on the sampling surface of the prism, the solvent was then injected into the cell and the selected solvent peak was recorded as a function of time. Data collection began when the solvent peak at 1056 cm^{-1} first appeared. Infrared intensities were measured with peak heights from the local baseline. Diffusion experiments ran from 2 to 10 h depending on the branch content of the samples and were conducted at room temperature.

Determination of the Diffusion Constants. To determine the diffusion constants, the infrared intensity at 1056 cm^{-1} from

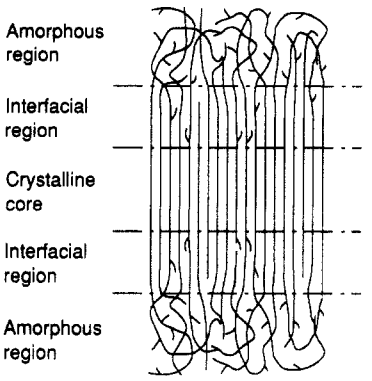

Figure 3. Model with three morphological regions proposed for ethyl-branched polyethylenes.[37] The ethyl side branches are distributed in the interfacial and amorphous regions and do not enter the crystalline core lattices.

the diffusant molecules at a measured time, $I(t)$, was normalized with respect to the infrared intensity of the same band at the saturation time, I_s, and the diffusion time was normalized with an arbitrary constant (in a unit of time). The normalized experimental data, as a function of time for the band, were then compared with those calculated from a Fickian diffusion model. Details of the calculation of the infrared response from the diffusant molecules can be found in ref 1. The time constant was then adjusted until the normalized experimental data best fit those calculated. The final chosen constant was converted to the diffusion constant using the relation, $D = (d_s^2)/(\text{constant})$, where d_s is the sampling depth. As discussed in ref 1, the sampling depth d_s can be taken as 3 times the penetration depth d_p. The penetration depth d_p, defined as the distance required for the electric field amplitude to fall to 1/e of its value at the interface in a sample film, is a function of the incident beam angle, the refractive indices of the ZnSe prism and the polymer film, and the absorption wavenumbers. With the present experimental conditions (i.e., the incident beam angle is 45°, the refractive indices of the prism and the polymer films are 2.4 and 1.52), the penetration depth and the sampling depth at 1056 cm^{-1} are approximately 2 and 6 μm, respectively.

Results

Crystallinity. The properties of the hydrogenated polybutadienes used in this work are shown in Table I. Note that sample crystallinities calculated from density measurements are higher than those determined from heat of fusion measurements. According to Mandelkern et al.[14-17,36] density measurements give larger degrees of crystallinity because they are sensitive to the interfacial regions (a model with three morphological regions proposed for ethyl-branched polyethylenes is shown in Figure 3). Increasing the number of ethyl branches along the polyethylene backbone decreases both the heat of fusion and the density of the samples, indicating a reduction in the crystallinity of the material. The differential scanning calorimeter (DSC) traces for samples with 6, 7, 11, and 24 branches/100 carbons are shown in Figure 4. A decrease in melting temperature and an increase in the width of the endothermic peak are evident as a result of increasing the branching content for the samples with 6, 7, and 11, branches/100 carbons. The endothermic peak is absent in the DSC trace for the sample with 24 branches/100 carbon backbones; instead, a broad exothermic peak is observed above the annealing temperature and the peak is maximized at around 120 °C. The melting temperature and the heats of fusion, as well as densities of our HPBD samples, are higher then those reported by Krigas et al.[38] We attribute this difference to different procedures in sample preparations. Krigas et al. samples were compression molded at 150 °C and quenched in ice water,

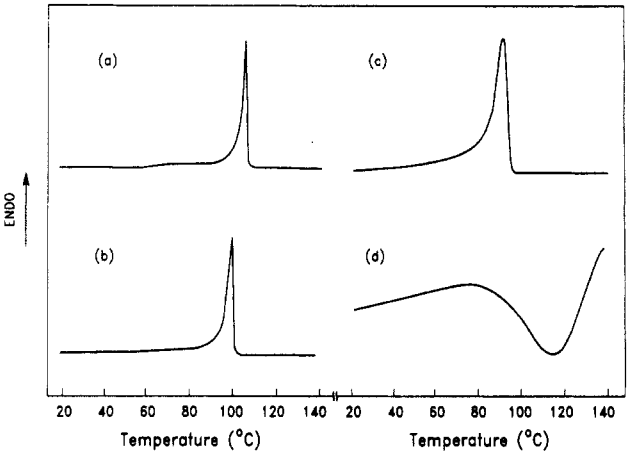

Figure 4. Differential scanning calorimeter (DSC) traces for samples with (a) 6, (b) 7, (c) 11, and (d) 24 branches/100 carbon backbones. The DSC trace for a highly branched sample shows an exothermic peak above the annealing temperature, whereas the less branched samples show endothermic peaks.

while in this work the samples were solution cast and annealed at 80 °C for 12 h. To erase sample preparation history, all samples were melted, followed by controlled cooling at 10 °C/min. A significant decrease in both heat of fusion and melting temperature was observed. Therefore, solution casting followed by annealing increased sample structural ordering, i.e., increased sample crystallinity. For the melted and then control-cooled sample with 24 branches/100 carbons, a smooth baseline was shown, which differs from the corresponding annealed sample, which exhibited a broad exothermic peak. The structure of the annealed samples with branches exceeding 24/100 carbons is not well understood at present; however, both DSC and density results show that the samples do not correspond to a fully relaxed amorphous phase. Densities for samples with 24 and 44 branches/100 carbons are 0.895 and 0.885 g/cm^3, while the pure amorphous densities for the corresponding samples are 0.863 and 0.869 g/cm^3, respectively. For highly branched samples, annealing may increase structural order as well, causing an increase in sample density. However, due to the large defects resulting from branching, it is reasonable to anticipate short-range ordering instead of long-range ordering, i.e., a partially ordered region instead of a crystalline core lattice. When highly branched samples are exposed to temperatures higher than the annealing temperature (80 °C), the short-range order increases, and the DSC trace shows an exothermic peak. This is consistent with Glotin and Mandelkern, who found that the contribution to the enthalpy from the partially ordered morphological region was either negligible or exothermic.[14]

Morphology. Parts a–d of Figure 5 are photomicrographs from the polarized optical microscopy study. Several morphological trends are seen from Figure 5a–d. First, for samples with 6, 7, and 11 branches/100 carbons, the size of aggregated crystallites decreased as the branch content increased, or more precisely, the crystalline texture became finer. This is because branches are excluded from the crystalline lattice, and they act as defects to prevent further growth of the crystallites. Second, a distribution of crystallites exists in each sample film; i.e., there are many large clusters of crystallites in the sample with 6 branches/100 carbons. As the branch number increases, the birefringence originates chiefly from the smaller crystallites and for the sample with 11 branches/100 carbons, there are no more large aggregated crystallites. A loss of crystal image contrast is also observed as the

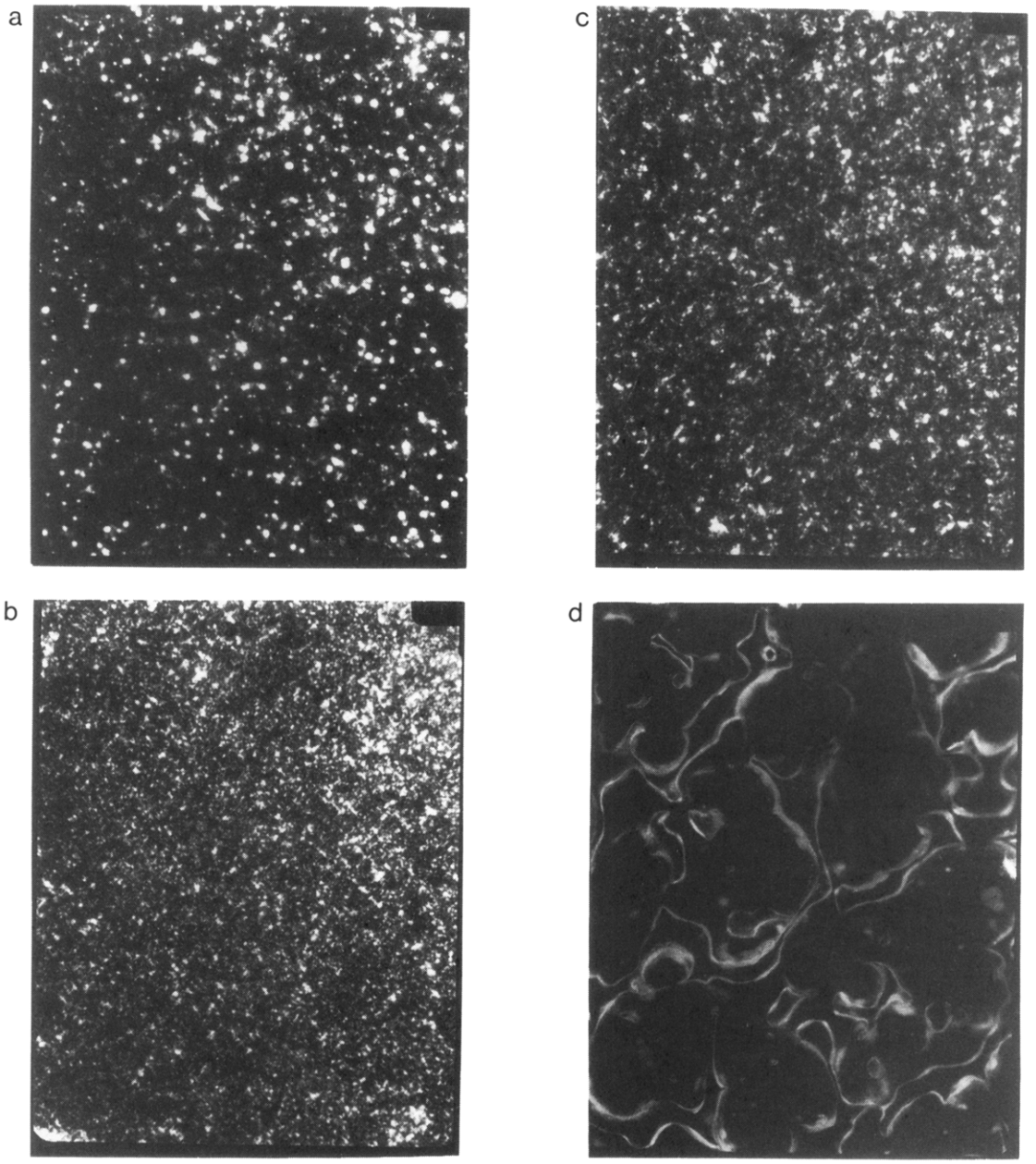

Figure 5. Photomicrographs from a polarized transmission optical microscope, which illustrate the length, shape, and distribution of the crystallites for HPBDs with (a) 6, (b) 7, (c) 11, and (d) 24 branches/100 backbone carbons. The photomicrographs were taken at a magnification of 200. (The figure scale is 50 μm/15.4 mm.) The polymer films were coated on a ZnSe ATR element.

branch number increased from 6 to 11 branches/100 carbons. Third, the photomicrographs reveal that the distribution of birefringent portion in the sample with 24 branches/100 carbons differs from those in the samples with 6, 7, and 11 branches/100 carbons. In the samples with 6, 7, and 11 branches/100 carbons, the birefringent portions are individual aggregated crystallites, while in the sample with 24 branches/100 carbons, the birefringent portions are large curved strips. A high degree of branching introduces large defects into the sample structure and prohibits the growth of the long-range order. It has been shown that ethyl branches do not enter the crystalline core[14,37,40] and that the minimum lamellar thickness of a crystalline core is 40 Å.[35] In other words, there should not be any crystalline lattices in highly branched samples. A further discussion of the detailed structure of highly branched samples will be presented in a later paper.

FTIR–ATR Measurements. Infrared spectra collected from the single reflection ATR liquid cell for the diffusion of *n*-decyl alcohol ($C_{10}OH$) into a HPBD sample with a branch number of 6/100 carbons are shown in Figure 6. The sample spectra exhibit a smooth baseline, indicating that the films were well attached to the sampling surface of the ATR element. The solvent peak at 1056 cm^{-1}, corresponding to the strong C–O stretching vibration in a primary alcohol, does not overlap peaks in the polymer spectra and was used to monitor the diffusion of $C_{10}OH$ into the HPBD samples. The broad solvent peak around 3300 cm^{-1} is consistent with solvent molecules existing as hydrogen-bonded dimers during the diffusion process. No absorption indicative of "free" O–H stretching at 3600–3650 cm^{-1} was observed.

Typical experimental spectra are shown in Figure 7. The peak intensity at 1056 cm^{-1} increases as a function of time, indicating the transport of $C_{10}OH$ into the polymer sample. Figure 8 is a plot of the infrared intensities of the peak at 1056 cm^{-1} as a function of time for the diffusion of $C_{10}OH$ into the various HPBD samples. Clearly, the number of ethyl side groups along the polyethylene backbone affects not only the diffusivity but also the

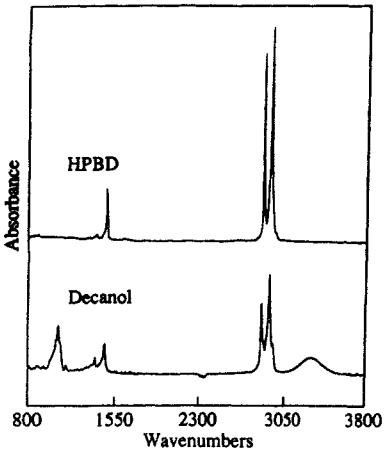

Figure 6. Infrared spectra collected from a single reflection ATR liquid cell for a hydrogenated polybutadiene sample with a branch number of 6/100 carbons (top) and *n*-decyl alcohol solvent (bottom).

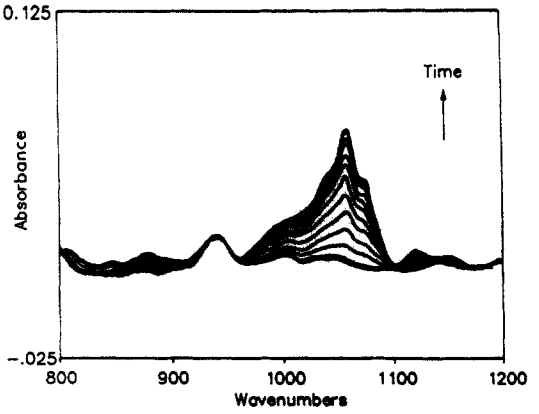

Figure 7. Selection of FTIR–ATR spectra of the diffusant (C_{10}OH) peak at 1056 cm^{-1} as a function of time (min) for the diffusion measurement of *n*-decyl alcohol into a polybutadiene sample with a branch number of 44/100 carbons. The peak at 1056 cm^{-1} is due to a strong C–O stretching vibration in a primary alcohol.

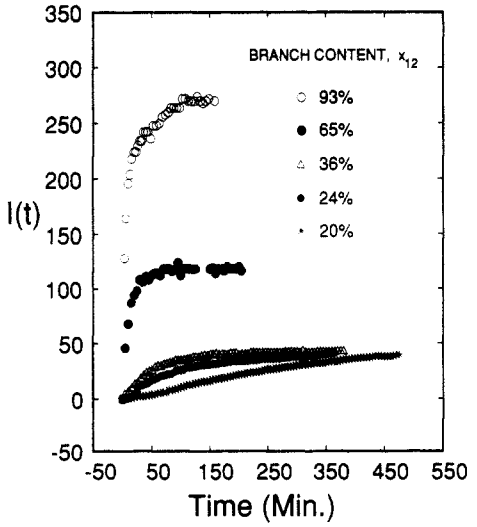

Figure 8. Infrared intensities of the solvent (C_{10}OH) peak at 1056 cm^{-1} as a function of time for diffusions of linear alcohol into varied branch content hydrogenated polybutadienes. Infrared intensities were measured with peak heights. The local baseline was used for peak height measurement.

solubility of C_{10}OH into ethyl-branched polyethylenes; i.e., an increase in branch content results in an increase in both diffusivity and solubility.

The saturation time, t_s, is the time from the first observation of the solvent peaks until it becomes constant

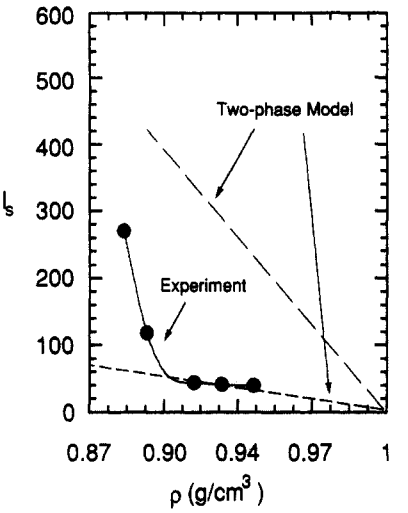

Figure 9. Equilibrium sorption values, I_s (arbitrary), as a function of the density of the HPBD samples. Data are from the *n*-decyl alcohol/polybutadiene diffusion system. The dashed lines represent the hypothetical equilibrium sorption behaviors based on a two-phase model.

in intensity. For classic Fickian-type diffusion, the saturation time is a measure of the rate of diffusion and is inversely proportional to the diffusion constant, while the infrared intensity at the saturation time is directly proportional to the solubility. The infrared intensities I_s at the saturation time are listed in Table I and are plotted as a function of the density ρ in Figure 9. A nonlinear dependence of the equilibrium sorption of C_{10}OH on the density of ethyl-branched polyethylene samples is observed. The equilibrium sorption is primarily affected by the relative amounts of the different regions in the samples. If one assumes a simple two-phase model where the samples consist of crystalline core and amorphous components only and the properties of the amorphous region are not affected by the existence of the crystallites, then the equilibrium sorption should be directly proportional to the density of the samples, as shown by the dashed lines. The short dashed line would lead to a confirmation of the simple two-phase model if there were no samples with densities lower than 0.900 g/cm^3, as in most other studies. The long dashed line represents a hypothetical simple two-phase model behavior by assuming an equilibrium sorption value for a completely amorphous sample. The nonlinear dependence of the sorption indicates that a simple two-phase model is not sufficient to explain the sorption behavior. The diffusion constants D are listed in Table I. For C_{10}OH diffusion into HPBDs, an exponential dependence of the diffusivities on the sample densities was found. The dependence of the ratio of D/D_a on the sample densities is plotted in Figure 10, where D_a is the diffusion constant in a completely amorphous sample. Model diffusion calculations have been performed for homogeneous distributions of impermeable crystallites with different shapes.[12,43,44] Among those, Frick's model[44]

$$\tau = 1 + [(1 - \alpha_a)/X]$$

where τ is the geometric impedance function, α_a is the amorphous fraction, and X is a constant for a given shape particle, gives the most realistic prediction and is plotted in Figure 10 along with the experimental data (in Figure 10, α_a has been converted to density). All these calculations uniformly yield a too weak dependence of the diffusion constant on crystallinity. Thus the experimentally observed geometric impedance is much higher than those

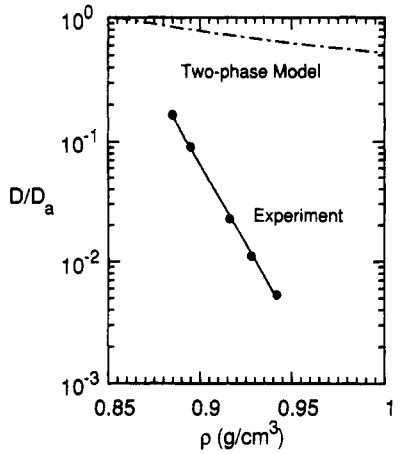

Figure 10. Diffusion constants, D (cm^2/s), as a function of the density of the HPBD samples. Data are from the *n*-decyl alcohol/polybutadiene diffusion system. The dashed line represents the predicted diffusion behavior based on Frick's two-phase model calculation.

derived from the impermeable crystallites alone in a simple two-phase model.

Discussion

Figures 9 and 10 point to clear shortcomings in the simple two-phase model. The source of disagreement with our data could come from several sources; here we consider three we feel most important. The first shortcoming is the assumption that the existence of the crystallites does not affect the properties of the amorphous region. As mentioned in the introduction, Michaels et al.[4] introduced a "chain immobilization factor" to account for the crystallite effect on the amorphous region in explaining their diffusion data. It is reasonable to anticipate that swelling, if it exists, would result in an increase in both the diffusion coefficient and the measured saturation intensity. Since crystallites act as cross-links and impede the swelling process, the extent of swelling decreases as crystallinity increases, because of the relative difficulty of the network to expand. We have shown that our diffusion curves match a classic Fickian model.[1,3] The classic Fickian model is based on the assumptions that no volume changes are associated with the movement of the penetrant and that the diffusion coefficients are constants. In reality, these assumptions do not hold and the classic Fickian model is inappropriate for swelling polymer systems. For systems in which the total amount of absorbed diffusants are small compared with the total mass of the polymer, the volume changes are small and the effect may not be too important, although not altogether negligible. During the diffusion process, we observed a slight decrease in the vibration bands of the polymer films, indicative of sample swelling, and the extent of swelling increased as the amorphous content increased. Thus, a modified model, including the swelling effect on the diffusion, may provide a better approach to our experimental data.

A second criticism of the two-phase model is that it does not account properly for the size, shape, and distribution of the crystallites. The deficiency of the two-phase model in modeling diffusion experiments may result from the assumption of a homogeneous dispersion of impermeable crystallites in an amorphous matrix. As the microscopy measurements show, there are birefringent regions in the sample with sizes much larger than individual crystals. Such aggregates of crystals may have larger geometrical impedance factors compared to homogeneous distributions, and models modified to account for such aggregates may better match our experimental data.

An obvious criticism of the two-phase model is that a linear combination of amorphous and crystalline portions is too simple a picture for semicrystalline polymers. It has been suggested that a boundary, or interphase, exists between lamellar crystallites and amorphous regions in semicrystalline polyethylenes, and recent experimental and theoretical developments indicate the presence of an interfacial region characterized by partial ordering of the chain units.[14-36] The existence of an intermediate structure in semicrystalline polymers would likely affect the transport properties. Since the ethyl groups do not enter the crystalline core and are distributed in the interfacial and amorphous regions, the interfacial region is expected to be less ordered than the crystalline core region and have a density between that of the amorphous and crystalline core regions. It has been shown experimentally that density measurements include a contribution from the interfacial region that is not reflected in the enthalpy of fusion measurements.[14-17,36,37,40] According to Mandelkern et al.[14-17,36] who determined the degree of crystallinity of ethylene copolymers by three different methods (enthalpy of fusion, density, and Raman internal modes), the values for crystallinity determined from heat of fusion and the core crystallinity determined from the Raman internal modes are nearly identical, and the degree of crystallinity determined from density measurements is the sum of the core crystallinity and interfacial content determined from the Raman spectroscopy. In principle, the fraction of interfacial region could be estimated from the difference of the crystallinity values determined from density and heat of fusion measurements, but since there is more than 50% uncertainty in the Raman measurements of the interfacial content,[15] a useful measure of the interfacial content cannot be obtained. Because of these limitations, a model with three morphological regions, an apparently more realistic picture of semicrystalline polymers, cannot be tested with our data. However, our experimental observations are in accord with three morphological regions. There is a significant difference in crystallinities determined by DSC and density measurements. For highly branched annealed samples, the crystalline core is likely to be absent; however, a short-range order or partially ordered region may still exist together with the amorphous region. The measured saturation intensities may be better interpreted in terms of a three morphological region model; i.e., at high branch contents, the saturation intensity continues to increase even though crystalline core is absent.

In addition to all the possible factors mentioned above that may affect the diffusion process, a rapid change in the polymer–solvent interactions at high branch contents, if it exists, would also cause a deviation from the simple two-phase model. Since the amorphous properties, as well as the solubility parameters for linear polyethylene (LPE) and poly(1-butene) (PB-1) are similar,[39] a dramatic change in the polymer–solvent interactions at high branch content seems unlikely. Moreover, since the amorphous density of poly(1-butene) is slightly higher than that of polyethylene,[38] the measured saturation intensity should be lower in poly(1-butene) than in linear polyethylene.

Conclusions

Hydrogenated polybutadienes (HPBDs) were characterized using FTIR, calorimetry, density, and optical microscopy techniques. A general decrease in structural ordering is observed with an increase in branch content. A marked difference in crystallinities determined by DSC

and density measurements was also evident, which is consistent with the presence of an interfacial region. In the highly branched annealed samples, it appears that the crystalline core is absent, but partial order is introduced into the samples during annealing.

The diffusive behavior of the *n*-decyl alcohol ($C_{10}OH$) dimer into the HPBD samples was investigated using a FTIR-attenuated total reflection sampling method. A nonlinear dependence of equilibrium sorption of $C_{10}OH$ on the density of the HPBDs was observed, indicating that a simple two-phase model is insufficient. An exponential dependence of diffusivities of $C_{10}OH$ on the density of the HPBDs was found and the observed geometric impedance is much larger than predicted from two-phase models. The presence of partial order may be the reason for the failure of the simple two-phase model in modeling equilibrium sorption and diffusion experiments. Other possible sources, such as sample swelling, the exclusion of modeling variables important to the diffusion process, like crystallite aggregation, or a rapid change in the polymer–solvent interactions at high branch contents, may also result in the disagreement of our data with the simple two-phase model.

Acknowledgment. The author would like to thank Dr. G. L. Baker, Dr. N. E. Schlotter, Dr. P. C. Warren, and Dr. T. N. Bowmer for their guidance, stimulating discussions, and helpful suggestions. Thanks also go to Dr. O. Gebizlioglu for his help with the optical microscopy.

References and Notes

(1) Schlotter, N. E.; Furlan, P. Y. *Vibr. Spectrosc.* **1992**, *3*, 147–153.
(2) Fujita, H. *Fortschr. Hochpolym.*—Forsch. **1961**, Ed. 3, S. 1–47.
(3) Schlotter, N. E.; Furlan, P. Y. *Polymer*, in press.
(4) Michaels, A. S.; Paker, R. B., Jr. *J. Poly,. Sci.* **1959**, *41*, 53.
(5) Michaels, A. S.; Bixler, H. J. *J. Polym. Sci.* **1961**, *50*, 391.
(6) Michaels, A. S.; Bixler, H. J. *J. Polym. Sci.* **1961**, *50*, 413.
(7) Peterlin, A. *J. Macromol. Sci., Phys.* **1975**, *B11* (1), 57–87.
(8) Billingham, N. C.; Calvert, P. D. In *The Physical Chemistry of Oxidation and Stabilization of Polyolefins*; Scott, G., Eds.; Developments in Polymer Stabilisation–3, Applied Science Publishers: London, 1980; Chapter 5.
(9) Rogers, C. E. In *Permeation of Gases and Vapours in Polymers*, Comyn, J., Eds.; Polymer Permeability; Elsevier Applied Science Published Ltd.: 1985; Chapter 2.
(10) Pospisil, J., Klemchuk, P. P., Eds. *Oxidation Inhibition in Organic Materials*; CRC Press, Inc.: Boca Raton, FL, 1990; Vols. 1 and 2.
(11) Muller-Plathe, F. *Chem. Phys. Lett.* **1991**, *177* (6), 527.
(12) Klute, C. H. *J. Appl. Polym. Sci.* **1959**, *1*, 340.
(13) Myers, A. W.; Rogers, C. E.; Stannett, V.; Szwarc, M. *Tappi* **1959**, *41*, 716.
(14) Glotin, M.; Mandelkern, L. *Colloid Polym. Sci.* **1982**, *260*, 182.
(15) Mandelkern, L. *Polym. J.* **1985**, *17*, 337.
(16) Alamo, R.; Domszy, R.; Mandelkern, L. *J. Phys. Chem.* **1984**, *88*, 6587–6595.
(17) Voigt-Martin, I. G.; Mandelkern, L. *J. Polym. Sci., Polym. Phys. Ed.* **1981**, *19*, 1769.
(18) Kitamaru, R.; Horii, F.; Hyon, S. H. *J. Polym. Sci., Polym. Phys. Ed.* **1977**, *15*, 821.
(19) Kitamaru, R.; Horri, F.; Murayama, K. *Macromolecules* **1986**, *19*, 636.
(20) Axelson, D. E.; Russell, K. E. *Prog. Polym. Sci.* **1985**, *11*, 221.
(21) Russell, T. P.; Ito, H.; Wignall, G. D. *Macromolecules* **1988**, *21*, 1703.
(22) Suzaki, H.; Grebowicz, J.; Wunderlich, B. *Macromol. Chem.* **1985**, *186*, 1109.
(23) Hahn, B.; Wendorff, J.; Yoon, D. Y. *Macromolecules* **1985**, *18*, 718.
(24) Hahn, B.; Herrmann-Schonherr, O.; Wendorff, J. H. *Polymer* **1987**, *28*, 201.
(25) Strobl, G. R.; Hagedorn, W. J. *J. Polym. Sci., Polym. Phys. Ed.* **1978**, *16*, 1181.
(26) Kunz, M.; Moller, M.; Heirich, U.-R.; Cantow, H. J. *Makromol. Chem., Makromol. Symp.* **1988**, *20–21*, 147; **1989**, *23*, 57.
(27) Flory, P. J. *J. Chem. Phys.* **1949**, *17*, 223.
(28) Flory, P. J. *J. Am. Chem. Soc.* **1962**, *84*, 2857.
(29) Mansfield, M. L. *Macromolecules* **1983**, *16*, 914.
(30) Flory, P. J.; Yoon, D. Y.; Dill, K. A. *Macromolecules* **1984**, *17*, 862.
(31) Yoon, D. Y.; Flory, P. J. *Macromolecules* **1984**, *17*, 868.
(32) Marqusee, J. A.; Dill, K. A. *Macromolecules* **1986**, *19*, 2420.
(33) Marqusee, J. A. *Macromolecules* **1989**, *22*, 472.
(34) Kumar, S. K.; Yoon, D. Y. *Macromolecules* **1989**, *22*, 3458.
(35) Alamo, R. G.; Mandelkern, L. *Macromolecules* **1989**, *22*, 1273.
(36) Mandelkern, L. *Acc. Chem. Res.* **1990**, *23*, 380–386.
(37) France, C.; Hendra, P. J.; Maddams, W. F.; Willis, H. A. *Polymer* **1987**, *28*, 710.
(38) Krigas, T. M.; Carella, J. M.; Struglinski, M. J.; Crist, B.; Graessley, W. W.; Schilling, F. C. *J. Polym. Sci., Polym. Phys. Ed.* **1985**, *23*, 509–520.
(39) Brandrup, J.; Immergut, E. H. *Polymer Handbook*, 3rd ed.; John Wiley and Sons: New York, 1989.
(40) Vile, J.; Hendra, P. J.; Willis, H. A.; Cudby, M. E. A.; Bunn, A. *Polymer* **1984**, *25*, 1173.
(41) Lowell, P. N.; MacCrum, N. G. *J. Polym. Sci. Lett.* **1967**, *5*, 1145.
(42) Lowell, P. N.; MacCrum, N. G. *J. Polym. Sci.* **1971**, *A2*, 1935.
(43) Runge, I. *Z. Tech. Phys.* **1925**, *6*, 61.
(44) Fricke, H. *Phys. Rev.* **1924**, *24*, 575.